Department of Chemical Engineering[1], Soongsil University; Samyang Biopharmaceuticals Corp.[2], Gyeonggi-do; Bio-Synectics, Inc.[3], Seoul, Republic of Korea

Dissolution enhancement of sorafenib tosylate by co-milling with tetradecanol post-extracted using supercritical carbon dioxide

I. Choi[1,#], S. Y. Park[2,#], S. -W. Lee[2], Z. Kang[3], Y. S. Jin[3], I. W. Kim[1,*]

Received July 10, 2019, accepted September 30, 2019

**Corresponding author: Il Won Kim, Department of Chemical Engineering, Soongsil University, Dongjak-gu, Seoul 06978, Republic of Korea*
iwkim@ssu.ac.kr
#These authors contributed equally to this work.

Pharmazie 75: 13-17 (2020) *doi: 10.1691/ph.2020.9120*

Sorafenib (SOR) is an important multikinase inhibitor for the treatment of cancers. It is commercially available (Nexavar from Bayer) in the form of sorafenib tosylate (SORt) due to its very low solubility. Studies have been made to further improve the dissolution behavior of the tosylate form (SORt), which could ultimately moderate the currently high daily dose. In the present study, SORt nanoparticles (SORt-NP) were prepared through a process that combined two industrially well-accepted techniques of co-milling and supercritical extraction. SORt was co-milled with hydrophilic polymers and tetradecanol, and the tetradecanol was post-extracted using supercritical carbon dioxide. The process enabled the formation of SORt-NP without using any toxic organic solvents, and the drug/excipient ratio (1:0.38) was substantially higher than determined in other studies (1:5.4–10). The enhanced dissolution behavior of SORt-NP was possible with an optimized number of milling cycles. Combining co-milling and supercritical extraction was able to form overall porous network structures with reduced crystallite size, which accelerated the dissolution of SORt-NP. The current method could be easily extended to other poorly soluble drugs as a general approach to improve their dissolution behaviors.

1. Introduction

Targeted therapy has been used to treat a wide spectrum of cancer, as it imparts relatively less damage to normal cells (Friedman and Ståhl 2009). Molecular-targeted drugs act as inhibitors of tumor growth and progression, performing on either tyrosine kinase receptors on cancer cell surfaces or serine/threonine kinases inside the cells (Martino et al. 2015). Sorafenib (SOR) is a multikinase inhibitor that blocks both the cell surface kinase receptors and intracellular kinases, which are related to tumor cell proliferation and angiogenesis (Wilhelm et al. 2004; Keating and Santoro 2009). It has been approved for the treatment of thyroid, renal cell, and unresectable hepatocellular carcinoma (Wilhelm et al. 2006; Escudier et al. 2007; Llovet et al. 2008; Liu et al. 2006).

SOR, however, is a Biopharmaceutics Classification System (BCS) class II molecule, having low aqueous solubility (25 ng/mL) (Wang et al. 2011). This results in low bioavailability with reduced sorafenib absorption in the gastrointestinal tract. In order to improve its solubility, a tosylate salt of sorafenib (SORt, Fig. 1) was developed (Nexavar®, Bayer HealthCare Pharmaceuticals–Onyx Pharmaceuticals, Leverkusen, Germany) (USFDA 2005). Although the solubility substantially increased (1.7–34.0 µg/mL in water at pH 1.0–4.5) (Nexavar: EPAR 2006), a relatively high daily dose of SORt is still required for effective therapy (400–800 mg/day) (USFDA 2005), which has been attributed to various side effects, such as diarrhea, nausea, anorexia, rash, and fatigue (Strumberg et al. 2007; Brose et al. 2014).

Diverse strategies have been presented to further increase the dissolution rate and ultimately bioavailability of SORt at the expense of high excipient addition. About 50-fold increase of SORt dissolution was observed in the presence of poly(vinylpyrrolidone-vinyl acetate) and sodium lauryl sulfate (Liu et al. 2016). Also, about 7-fold increase of bioavailability was shown with the use of organic additives combined with mesoporous silica or lipid-coated nanodiamond (Gua et al. 2017; Zhang et al. 2014).

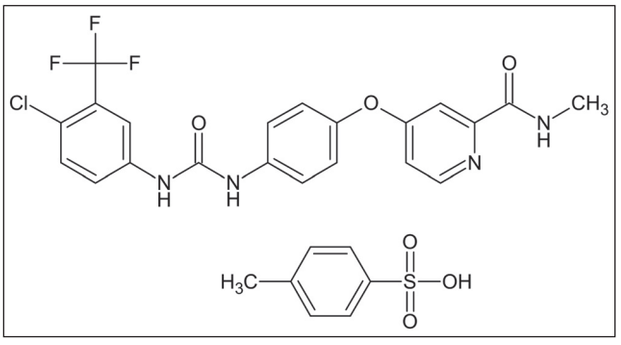

Fig. 1: Chemical structure of SORt.

Nevertheless, large amounts of excipients are used in these studies, excipient/SORt (w/w) = 5.4–10, which means a low loading of SORt and elevated preparation costs. Also, various organic solvents (methanol, ethanol, and dichloromethane) were utilized during the preparation steps (Gua et al. 2017; Zhang et al. 2014). Unfortunately, the large quantities of excipients and the use of organic solvents appear to be related to the undesirable increase of toxicity (Brose et al. 2014; Mirmoghaddam et al. 2015).

The purpose of the present study was to enhance the dissolution rate of SORt through the formation of novel SORt nanoparticles (SORt-NP), with a substantially reduced amount of excipients (i.e., high SORt loading). SORt-NP powders were prepared by co-milling SORt and hydrophilic polymers in the presence of a solid lipid (tetradecanol) that was post-extracted by supercritical carbon dioxide. Co-milling of hydrophobic drugs and hydrophilic polymers has been investigated to improve the dissolution rate of the sparingly soluble drugs, and the improvement was presumably due to the particle-size decrease and the wettability increase

(Sugimoto et al. 1998; Garg et al. 2009). In the present study, the improved dissolution rate of the SORt-NP was observed in fasted-state simulated gastric fluid (FaSSGF), and it was correlated with the various structural features of SORt-NP regulated by the process parameters.

2. Investigations, results and discussion

2.1. Preparation of SORt-NP

SORt-NP was prepared by incorporating SORt into the matrix lipid, TD, which was removed after milling to leave SORt as the size-reduced particles. TD was selected as the matrix lipid, because its low melting point (39 ºC) was in the range that could facilitate its removal by supercritical carbon dioxide. SORt/TD weight ratio was 1:3, which was found efficient to prevent the phase transformation between SORt polymorphs (from III to form I) that could be caused by the heat generated during milling (data not shown). Also, TD was expected to protect the active ingredient against chemical or physical degradation during the milling process (Dingler et al. 1999).

In addition, HPMC, PVP, and P407 were selected as dissolution-enhancing excipients and stabilizers (Sugimoto et al. 1998; Ghosh et al. 2011). In order to determine the optimal compositions of SORt-NP formulation, separate screening studies were conducted using Design of Experiment (DoE) affiliated in Quality by Design (QbD) approach (Park et al. 2019). In brief, DoE was employed with Box-Behnken design using Design-Expert and MODDE® software (Venugopal et al. 2016; Singare et al. 2010; Patel et al. 2014). A total of fifteen experiments were carried out to study the different ratios of excipients to SORt affecting the particle size, the peak concentration (C_{max}), and area under the concentration-time curve (AUC) of SORt. The results indicated that the optimum weight ratio was HPMC/PVP/P407/SORt = 0.25:0.1:0.03:1.

In the present study, the main focus was to find the optimal number of milling cycles. Milling with the roller compactor was performed at 2, 4, 8, 12, 14, and 18 cycles to evaluate the effect of the degree of milling on the structure-property relationships of SORt-NP. The SORt-NP produced at milling cycles of 2, 4, 8, 12, 14, and 18 were named RM2, RM4, RM8, RM12, RM14, and RM18, respectively. Details of the SORt-NP characterization are presented in the following section.

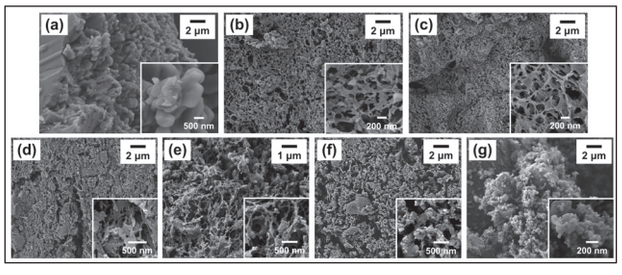

Fig. 2: SEM micrographs of (a) SORt (raw material as received); (b) RM2; (c) RM4; (d) RM8; (e) RM12; (f) RM14; (g) RM18. RM2 through RM18 are SORt-NP processed through milling and extraction, numeral being the number of milling cycles.

2.2. Characterization of SORt-NP

Morphologies of SORt and SORt-NP were observed with FE-SEM, and summarized in Fig. 2. SORt was observed as received, and SORt-NP was examined after TD removal. SORt was present as aggregated granules (Fig. 2a), and the individual granule was approximately 2 µm in size (see the Figure insert). SORt-NP from RM2 to RM12 exhibited interconnected porous structures as shown in Fig. 2b to 2e. The fraction of the porous region was measured for representative 2 × 2 µm regions using Image J software, and it was 28%, 30%, 28%, and 38% for RM2, RM4, RM8 and RM12, respectively. The porous structures were most likely the result of the TD removal by supercritical CO_2 when SORt and excipient polymers had been well dispersed in the matrix-like TD. The increase of the porous region up to RM12 indicated that the close incorporation of the polymeric excipients and SORt and their dispersion in TD were in progress being complete up to the twelfth milling cycle. Before the twelfth milling cycle, the incorporation and the dispersion seemed incomplete. In contrast, RM14 appeared mostly clustered particles, while some porous regions were still visible (Fig. 2f). As the number of milling cycles increased to generate RM18, porous structure was no longer identifiable, and only the agglomerated clusters were observed (Fig. 2g). The formation of the agglomerated clusters evidenced that phase separation of the constituent materials occurred, which undoubtedly disrupted the formation process of the porous network structure. The origin of this behavior was probably related to the increase of the local temperature with excessive milling that enabled TD to provide a fluid environment for the phase separation because of its low melting point (39 ºC).

The increased mechanical energy with excessive milling cycles translating into the locally elevated temperature of the milled compounds was substantiated by the reduced water content measured after milling (before drying and TD removal). The water content measured by Karl Fischer titration method was 14.7%, 12.4%, 6.6%, 5.5%, 3.1%, and 0.8% for RM2, RM4, RM8, RM12, RM14, and RM18, respectively. Also, for the roller compactor employed in the current study, water content less than 5% often caused problematic overloading. Overall, the constraint in the milling process appeared to counterbalance the efficacy of dispersion when the number of cycles was over 12, and the morphological changes with the excessive milling cycles were closely related to the process conditions inferred by the water content.

The hydrodynamic particle size and PDI of SORt-NP were evaluated by light scattering after powders were sonicated in DI water for 30 sec to disperse loose agglomerates (Table 1). The particle size decreased proportional to the number of milling cycles, from about 610 nm for RM2 to 390 nm for RM18. Also, PDI values were between 0.2 and 0.3 for RM2 through RM14 where at least some porous network structures were visible during SEM observations, and it became less than 0.1 for RM18 when porous structure disappeared completely. (Note that PDI value 0 is equivalent to the monodisperse size distribution.) Overall, the results of DLS measurements appeared to correlate well with the SEM observations, and confirmed the effectiveness of the milling process at the level of apparent particle size.

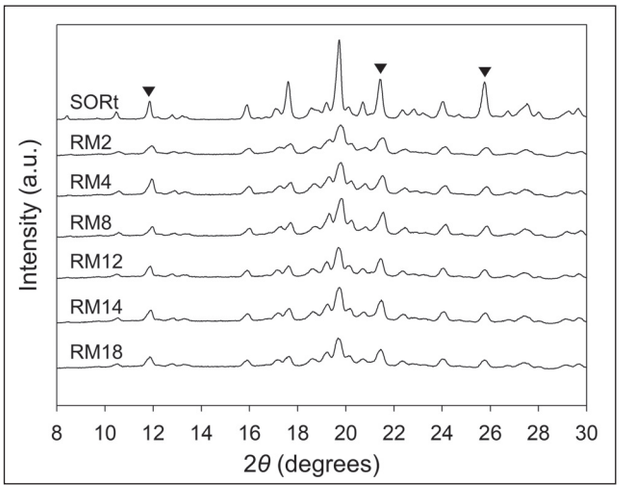

Fig. 3: XRD patterns of SORt and SORt-NP prepared with different milling cycles (RM2, RM4, RM8, RM12, RM14, and RM 18).

XRD analysis was performed to determine the crystal structures of SORt-NP (Fig. 3). First, diffraction patterns of SORt-NP and SORt were nearly identical in the peak positions, confirming no change in the crystal polymorph after the process to generate SORt-NP from SORt (form III). Second, the diffraction peaks of SORt-NP were

Table 1: Hydrodynamic size and PDI of SORt-NP prepared with different milling cycles

SORt-NP	RM2	RM4	RM8	RM12	RM14	RM18
Hydrodynamic size[a] (nm)	606.1±42.6	527.4±42.1	468.1±31.7	440.8±28.8	407.9±29.3	394.5±9.9
PDI	0.26	0.27	0.24	0.25	0.23	0.09

[a] mean ± standard deviation (n = 3)

broadened compared to those of SORt. The changes were quantified through the analysis using the Scherrer equation (Scherrer 1918):

$$L = \frac{K\lambda}{\beta cos\theta}$$

where L is the crystallite size, λ is the wavelength of X-ray (λ = 1.5406 Å), θ is the diffraction angle, β is the full width at half maximum (FWHM) of the diffraction peak, and K is a constant related to crystallite shape and generally taken as 0.9. The prominent peaks at 11.9°, 21.4° and 25.8° (marked ▼) were used because of their clear separation from nearby diffraction peaks, and the results were shown in Table 2. The crystallite size of all SORt-NP was less than that of SORt, indicating the decrease was the result of the milling process. The size decreased proportionally to the number of milling cycles up to RM12, and increased for RM14 and RM18. The observed phenomena could be interpreted as the efficient milling (comminution) counterbalanced by the overloading-related complication (RM14 and RM18) verified by monitoring the morphology and water content of SORt-NP. During the overloading, excess mechanical energy combined with heating could form an environment that instigated the growth of the crystallite. TD has the melting point (39 ºC) near room temperature, and slight local heating is probably enough to make it solvent-like for SORt. This would lower the activation energy for the crystal ripening to expedite the process of crystallite growth. Note that the process of crystallite growth appeared intimately related to the phase separation of the milled materials and the disruption of the porous network structure, as described for Fig. 2.

Table 2: Crystallite size calculated from the XRD patterns of SORt and SORt-NP prepared with different milling cycles

2θ	Crystallite size (nm)						
	SORt	RM2	RM4	RM8	RM12	RM14	RM18
11.9°	44.4	33.3	30.7	26.6	26.6	33.3	33.3
21.4°	33.7	27.0	27.0	25.3	20.2	22.5	25.3
25.8°	31.4	29.1	27.2	25.5	22.6	24.0	25.5

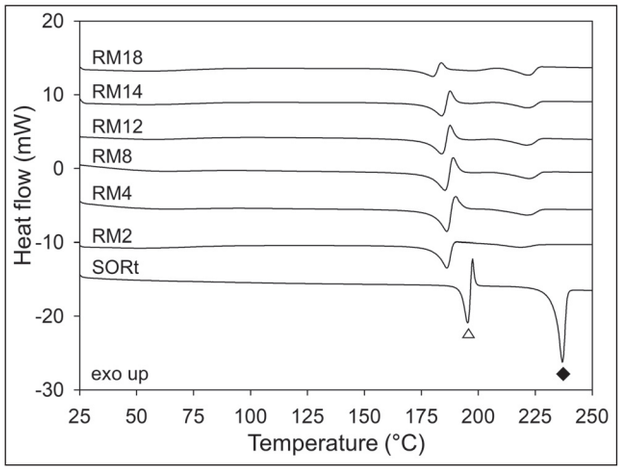

Fig. 4: DSC thermograms of SORt and SORt-NP prepared with different milling cycles (RM2, RM4, RM8, RM12, RM14, and RM 18).

Thermal properties of the SORt-NP were investigated with DSC, and their thermograms were compared with that of SORt in Fig. 4. For SORt, there were two endotherms at 195 ºC (marked Δ) and 237 ºC (marked ♦), and additional exotherm right after the first endotherm. The former endotherm was related to the melting of form III, after which form I of the higher melting point was immediately recrystallized and eventually melted (Grunenberg and Lenz 2006). Also for SORt-NP, the overall behavior (one exotherm flanked by two endotherms) was preserved but with the substantial reduction of the melting points. First endothermic peaks of the nanoparticles were in the range 180–186 ºC and second endothermic peaks were at ca. 222 °C. They were about 9–15 °C and 15 °C lower than those of SORt, respectively. The melting point depression was probably due to the incorporation of polymeric excipients, decreasing the chemical potential of the drug in the mixture (Marsac and Li 2009).

Dissolution behaviors of SORt, SOR, and SORt-NP are compared in Fig. 5. In general, dissolution was in the order SORt-NP (RM series) > SORt > SOR. Especially enhanced dissolution behaviors were observed for RM8 and RM12, whereas that of RM18 was the worst among all the SORt-NP cases. The successful dissolution increase of RM8 and RM12 could be attributed to the both the presence of porous network structures (Fig. 2) and the decrease of the crystallite size (Table 2). Both could contribute the large surface area that increased the dissolution rate (Noyes and Whitney 1897), the former to the initially large surface area and the latter to the surface area at the later stage. In contrast, RM18 lacked the porous structure and its crystallite size was relatively larger, although its apparent hydrodynamic size was smaller than any other SORt-NP (Table 1).

Another significant difference of RM18 from other SORt-NP was the notable decrease of concentration after 100-min dissolution, which resembled the behavior of SORt converging to the SOR profile. The converged profiles of SORt and SOR suggested the precipitation of SOR at the later stage, even when SORt was the initial form of dissolution. The fact that only RM18 displayed similar behavior indicated that the SORt in RM18 was less protected by the polymeric additives than that in other SORt-NP probably because of the poor dispersion related to the overloading problem. Note that RM2 with minimal milling started to show such behavior after 200-min dissolution but not as extensively as RM18.

2.3. Conclusions

In summary, SORt-NP was prepared by a technique that combined milling and supercritical extraction. Milling SORt and excipients (HPMC, PVP, and P407) in the presence of TD matrix was followed by the removal of TD using supercritical CO_2. Our aim was to optimize the number of milling cycles by correlating the structures of SORt-NP with its dissolution behavior. The governing factors that increased the dissolution behavior were the presence of porous network structures and the decrease of crystallite size. These were most prominent for the SORt-NP with twelve milling

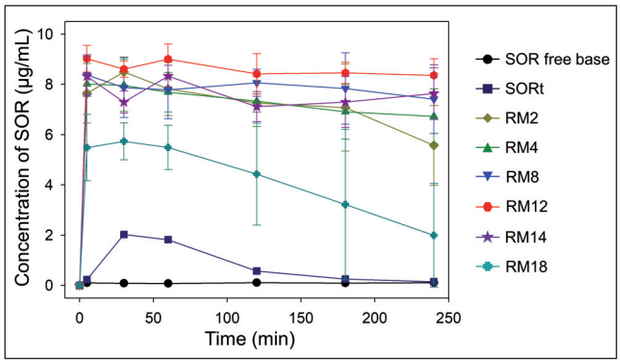

Fig. 5: In vitro dissolution profiles (FaSSGF, n = 3) of SORt-NP prepared with different milling cycles (RM2, RM4, RM8, RM12, RM14, and RM 18) compared with SORt and SOR.

cycles (RM12) within the limit of current experimental conditions, and its dissolution was most enhanced (about four times of control SORt). Further increase of milling cycle deteriorated the porous structure and increased the crystallite size, which translated into the decrease of the dissolution rate, even when the conventional particle size measured by dynamic light scattering became smaller. We also note that the current technology distinguishes itself from other methods in that no toxic organic solvent is used in all procedures and the use of excipients is minimal (i.e., high loading of SORt), excipient/SORt (w/w) = 0.38 compared to 5.4–10 in other studies (Liu et al. 2016; Gua et al. 2017; Zhang et al. 2014). We believe that the current technology that combines two industrially well-accepted processes could be extensively applied to the poorly soluble drugs to improve their dissolution behaviors with high drug/excipient ratios.

3. Experimental

3.1. Materials

Sorafenib tosylate (SORt: form III, 99.6%) was purchased from Hetero Labs (Hyderabad, India), its chemical structure is shown in Fig. 1. Sorafenib (SOR: free base, 99.4%) was purchased from Jinan Rouse Industry Co. (Jinan, China). Hydroxypropyl methylcellulose (HPMC: METHOCEL™ E5 Premium LV, 85-99%) was purchased from Dow Chemical Korea (Seoul, Korea). Polyvinylpyrrolidone (PVP: Kollidon® 30, M_w 44,000-54,000 g/mol), poloxamer 407 (P407: Kolliphor® P407, M_w 9,840-14,600 g/mol), and 1-tetradecanol (TD) were purchased from BASF (Ludwigshafen, Germany). Deionized (DI) water was obtained from Pure RO-I (Human Science, Hanam, Korea). Fasted-state simulated gastric fluid (FaSSGF, sodium taurocholate 80 μM, lecithin 20 μM, pepsin 0.1 mg/mL, and sodium chloride 34.2 mM) powder was purchased from Biorelevant (Surrey, UK). Acetonitrile (HPLC grade) was purchased from Honeywell Burdick & Jackson (Muskegon, MI, USA).

3.2. Preparation of SORt-NP

SORt, HPMC, PVP, P407, TD, and DI water were charged in a beaker and physically mixed. The addition was at the weight ratios SORt/TD/DI water = 1:3:0.75 and SORt/HPMC/PVP/P407 = 1:0.25:0.1:0.03. The mixture was then milled using a roller compactor (Intech System, Hanam, Korea) with different number of milling cycles (2, 4, 8, 12, 14, and 18). This process was to homogenize the mixture thoroughly and reduce the particle size of SORt. After milling, water content of the mixture was measured, since too low water content could cause the processing problem of compactor overloading. Karl Fischer titration method (Volumetric KF Titrator V20, Mettler-Toledo, Columbus, OH, USA) was utilized with 100 mg of milled sample. The milled sample was eventually dried under vacuum to obtain powder, of which TD was subsequently removed with flowing supercritical CO_2 using a supercritical fluid system (Bio-Synectics, Seoul, Korea) (Park et al. 2013; Kim and Cho 2007). The resulting SORt-NP powders were named as RM2, RM4, RM8, RM12, RM14, and RM18, depending on the number of milling cycles.

3.3. Solid-state characterization

Morphologies of SORt (raw material as received) and SORt-NP (after processing) were observed through field-emission scanning electron microscopy (FE-SEM: SIGMA, Carl Zeiss, Oberkochen, Germany) after thin Au coating using a sputter coater (EM ACE200, Leica, Wetzlar, Germany). Image J software (National Institutes of Health, Bethesda, MD, USA) was used to analyze the SEM images.

Crystal structures were studied with X-ray diffraction (XRD: D8 PHASER, Bruker AXS, Billerica, MA, USA). XRD was performed with CuKα radiation (λ = 1.5406 Å) at 30 kV and 10 mA in 2θ region of 6–40º with a scanning rate of 1º/min. A Si low-background sample holder (Bruker AXS, Billerica, MA, USA) was used.

Thermal properties were investigated using differential scanning calorimetry (DSC: DSC3 STAR^e system, Mettler-Toledo, Columbus, OH, USA). DSC was pre-calibrated for enthalpy and temperature using indium. For each sample, about 2–3 mg powder was weighed in a 40 μL aluminum pan with a pinhole-punched lid. The scanning was from 25 to 250 ºC with a heating rate of 10 ºC/min under nitrogen gas atmosphere.

Particle size and polydispersity index (PDI) of SORt-NP in aqueous dispersion were determined through dynamic light scattering (DLS: ELSZ-1000, Otsuka electronics Co., Osaka, Japan). For each SORt-NP, powder 10 mg was suspended in DI water (10 mL) and dispersed for 30 s under ultrasonication (WUC-A01H, DAIHAN Scientific Co., Seoul, Korea). After dispersion, ca. 1 mL was used for the DLS experiment. All measurements were repeated in triplicate.

3.4. Dissolution study

In vitro release behaviors of SOR, SORt, and SORt-NP were studied in FaSSGF (pH 1.6) using a USP type II apparatus (paddle) at 75 rpm. The FaSSGF was prepared following the instructions of the supplier, and contained sodium taurocholate (80 μM), lecithin (20 μM), pepsin (0.1 mg/mL), and sodium chloride (34.2 mM). For each measurement, powder (222 μg/mL as SOR) was placed in a 900 mL FaSSGF solution at 37 ºC. The 3 mL aliquots of the solution were withdrawn after 5, 30, 60, 120, 180, and 240 min, and the solution was immediately replenished with 3 mL of the fresh dissolution medium to maintain the total volume constant. The aliquots were filtered through 0.22 μm PTFE syringe filters and analyzed using a high performance liquid chromatography system (HPLC: Shimadzu Co., Kyoto, Japan) equipped with a Phenomenex Luna C18 column (5 μm, 250 × 4.6 mm, Phenomenex, Torrance, CA, USA). The composition of the mobile phase was acetonitrile/water = 82.5:17.5 (v/v). The flow rate was 1.5 mL/min, and the injection volume was 20 μL. UV detection for the concentration determination was carried out at wavelength 265 nm (SPD-20A UV-visible detector, Shimadzu Co., Kyoto, Japan). All measurements were repeated in triplicate, and no degradation of SOR was observed.

Acknowledgments: This work was supported by the Technology R&D Project (10067366, The improvement of dosage regimen and administration of targeted anticancer drugs by using nano-powderization technology) funded by the Ministry of Trade, Industry & Energy (MOTIE, Korea) and Basic Science Research Program through the National Research Foundation of Korea (NRF) funded by the Ministry of Education (NRF- 2015R1D1A1A01058116).

Conflicts of interest: None declared.

References

Brose MS, Frenette CT, Keefc SM, Stein SM (2014) Management of sorafenib-related adverse events: a clinician's perspective. Semin Oncol 41(supplement 2): S1-S16.

Dingler A, Blum RP, Niehus H, Müller RH, Gohla S (1999) Solid lipid nanoparticles (SLN™/Lipopearls™)- a pharmaceutical and cosmetic carrier for the application of vitamin E in dermal products. J Microencapsul 16: 751-767.

Escudier B, Eisen T, Stadler WM, Szczylik C, Oudard S, Siebels M, Negrier S, Chevreau C, Solska E, Desai AA, Rolland F, Demkow T, Hutson TE, Gore M, Freeman S, Schwartz B, Shan M, Simantov R, Bukowski RM (2007) Sorafenib in advanced clear-cell renal-cell carcinoma. N Engl J Med 356: 125-134.

Friedman M, Ståhl S (2009) Engineered affinity proteins for tumour-targeting applications. Biotechnol Appl Biochem 53: 1-29.

Garg A, Singh S, Rao VU, Bindu K, Balasubramaniam J (2009) Solid state interaction of raloxifene HCl with different hydrophilic carriers during co-grinding and its effect on dissolution rate. Drug Dev Ind Pharm 35: 455-470.

Ghosh I, Bose S, Vippagunta R, Harmon F (2011) Nanosuspension for improving the bioavailability of a poorly soluble drug and screening of stabilizing agents to inhibit crystal growth. Int J Pharm 409: 260-268.

Grunenberg A, Lenz J (2006) Thermodynamically stable form of BAY 43-9006 tosylate. WO/2006/034797.

Gua Y, Zhong T, Duan XC, Zhang S, Yao X, Yin YF, Huang D, Ren W, Zhang Q, Zhang X (2017) Improving anti-tumor activity of sorafenib tosylate by lipid- and polymer-coated nanomatrix. Drug Deliv 24: 270-277.

Keating GM, Santoro A (2009) Sorafenib: a review of its use in advanced hepatocellular carcinoma. Drugs 69: 223-240.

Kim K, Cho Y (2007) Method for preparing nano-scale particle of active material. WO/2007/129829.

Liu C, Chen Z, Chen Y, Lu J, Li Y, Wang S, Wu G, Qian F (2016) Improving oral bioavailability of sorafenib by optimizing the "spring" and "parachute" based on molecular interaction mechanisms. Mol Pharm 13: 599-608.

Liu L, Cao Y, Chen C, Zhang X, McNabola A, Wilkie D, Wilhelm S, Lynch M, Carter C (2006) Sorafenib blocks the RAF/MEK/ERK pathway, inhibits tumor angiogenesis, and induces tumor cell apoptosis in hepatocellular carcinoma model PLC/PRF/5. Cancer Res 66: 11851-11858.

Llovet JM, Ricci S, Mazzaferro V, Hilgard P, Gane E, Blanc JF, De Oliveira AC, Santoro A, Raoul JL, Forner A, Schwartz M, Porta C, Zeuzem S, Bolondi L, Greten TF, Galle PR, Seitz JF, Borbath I, Häussinger D, Giannaris T, Shan M, Moscovici M, Voliotis D, Bruix J (2008) Sorafenib in advanced hepatocellular carcinoma. N Engl J Med 359: 378-390.

Marsac PJ, Li T, Taylor LS (2009) Estimation of drug-polymer miscibility and solubility in amorphous solid dispersions using experimentally determined interaction parameters. Pharm Res 26: 139-151.

Martino SD, Rainone A, Troise A, Paolo MD, Pugliese S, Zappavigna S, Grimaldi A, Valente D (2015) Overview of FDA-approved anticancer drugs used for targeted therapy. WCRJ 2: e553.

Mirmoghaddam M, Kaykhaii M, Yahyavi H (2015) Recent developments in the determination of residual solvents in pharmaceutical products by microextraction methods. Anal Methods 7: 8511-8523.

Nexavar: European Public Assessment Reports (EPAR)-Scientific Discussion. European Medicines Agency (EMA). (2006) Available from: http://www.ema.europa.eu/docs/en_GB/document_library/EPARScientific_Discussion/human/000690/WC500027707.pdf.

Noyes AA, Whitney WR (1897) The rate of solution of solid substances in their own solutions. J Am Chem Soc 19: 930–934.

Park JW, Yun JM, Lee ES, Youn YS, Kim KS, Oh YT, Oh KT (2013) A nanosystem for water-insoluble drugs prepared by a new technology, nanoparticulation using a solid lipid and supercritical fluid. Arch Pharmacal Res 36: 1369-1376.

Park SY, Kang Z, Thapa P, Jin YS, Park JW, Lim HJ, Lee JY, Lee SW, Seo MH, Kim MS, Jeong SH (2019) Development of sorafenib loaded nanoparticles to improve oral bioavailability using quality by design approach. Int J Pharm 566: 229-238.

Patel GV, Patel VB, Pathak A, Rajput SJ (2014) Nanosuspension of efavirenz for improved oral bioavailability: formulation optimization, in vitro, in situ and in vivo evaluation. Drug Dev Ind Pharm 40: 80-91.

Scherrer P (1918) Bestimmung der Grösse und der inneren Struktur von Kolloidteilchen mittels Röntgenstrahlen, Nachrichten von der Gesellschaft der Wissenschaften. Göttingen Math Phys 2: 98-100.

Singare DS, Marella S, Gowthamrajan K, Kulkarni GT, Vooturi R, Rao PS (2010) Optimization of formulation and process variable of nanosuspension: an industrial perspective. Int J Pharm 402: 213-220.

Strumberg D, Clark JW, Awada A, Moore MJ, Richly H, Hendlisz A, Hirte HW, Eder JP, Lenz HJ, Schwartzh B (2007) Safety, pharmacokinetics, and preliminary antitumor activity of sorafenib: a review of four phase I trials in patients with advanced refractory solid tumors. Oncologist 12: 426-437.

Sugimoto M, Okagaki T, Narisawa S, Koida Y, Nakajima K (1998) Improvement of dissolution characteristics and bioavailability of poorly water-soluble drugs by novel cogrinding method using water-soluble polymer. Int J Pharm 160: 11-19.

US Food and Drug Administration. FDA approval for sorafenib tosylate (Nexavar®). (2005) Available from: https://www.accessdata.fda.gov/drugsatfda_docs/label/2010/021923s008s009lbl.pdf.

Venugopal V, Kumar KJ, Muralidharan S, Parasuraman S, Raj PV, Kumar KV (2016) Optimization and in-vivo evaluation of isradipine nanoparticles using Box-Behnken design surface response methodology. OpenNano 1: 1-15.

Wang XQ, Fan JM, Liu YO, Zhao B, Jia ZR, Zhang Q. (2011) Bioavailability and pharmacokinetics of sorafenib suspension, nanoparticles and nanomatrix for oral administration to rat. Int J Pharm 419: 339-346.

Wilhelm S, Carter C, Lynch M, Lowinger T, Dumas J, Smith RA, Schwartz B, Simantov R, Kelly S (2006) Discovery and development of sorafenib: a multikinase inhibitor for treating cancer. Nat Rev Drug Discov 5: 835-844.

Wilhelm SM, Carter C, Tang L, Wilkie D, McNabola A, Rong H, Chen C, Zhang X, Vincent P, McHugh M, Cao Y, Shujath J, Gawlak S, Eveleigh D, Rowley B, Liu L, Adnane L, Lynch M, Auclair D, Taylor I, Gedrich R, Voznesensky A, Riedl B, Post LE, Bollag G, Trail PA (2004) BAY 43-9006 exhibits broad spectrum oral antitumor activity and targets the RAF/MEK/ERK pathway and receptor tyrosine kinases involved in tumor progression and angiogenesis. Cancer Res 64: 7099-7019.

Zhang Z, Niu B, Chen J, He X, Bao X, Zhu J, Yu H, Li Y (2014) The use of lipid-coated nanodiamond to improve bioavailability and efficacy of sorafenib in resisting metastasis of gastric cancer. Biomaterials 35: 4565-4572.